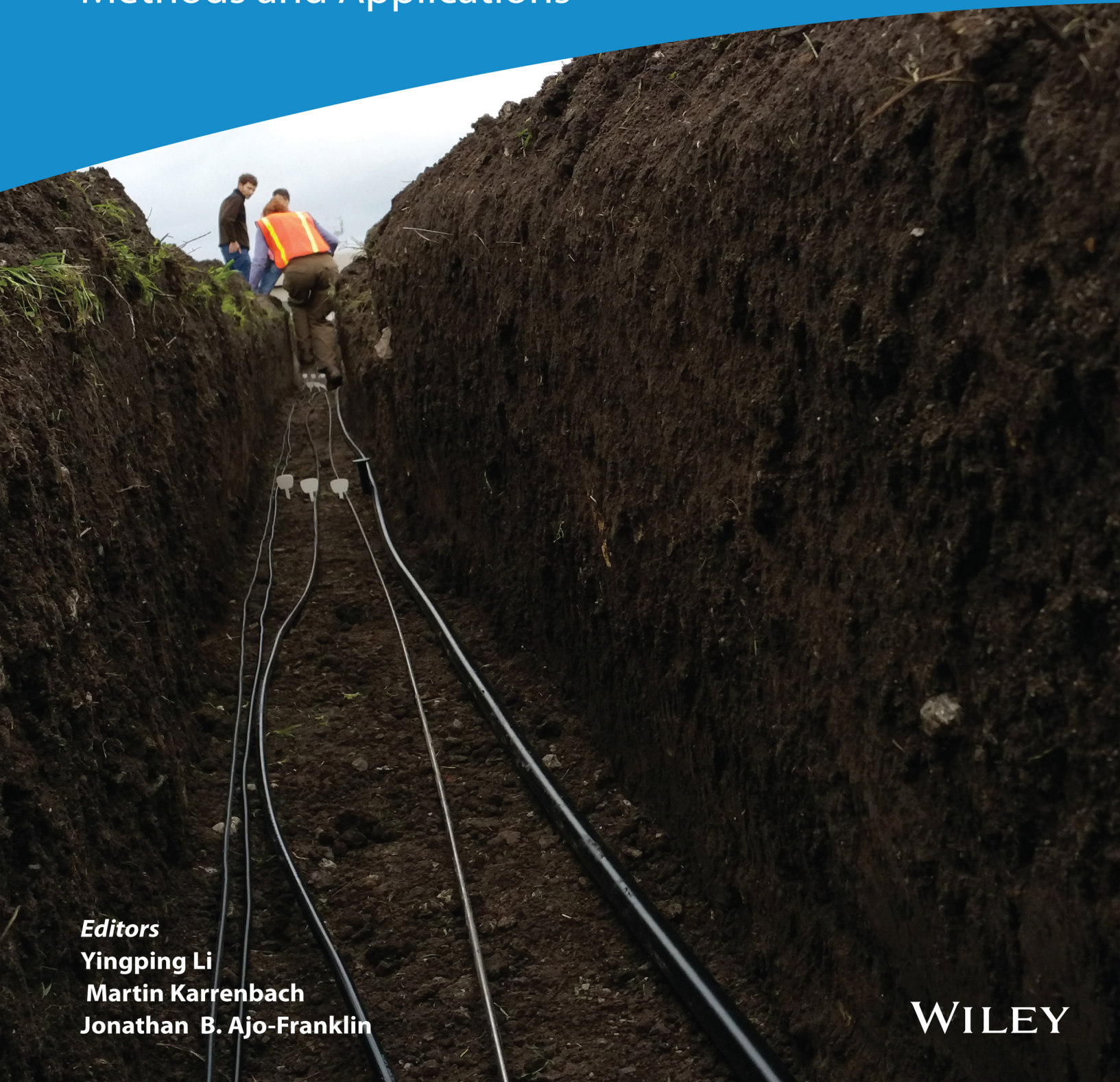


GEOPHYSICAL MONOGRAPH SERIES

AGU
ADVANCING EARTH
AND SPACE SCIENCE

Distributed Acoustic Sensing in Geophysics

Methods and Applications



Editors

Yingping Li

Martin Karrenbach

Jonathan B. Ajo-Franklin

WILEY

Geophysical Monograph Series

Geophysical Monograph Series

- 212 **The Early Earth: Accretion and Differentiation** *James Badro and Michael Walter (Eds.)*
- 213 **Global Vegetation Dynamics: Concepts and Applications in the MC1 Model** *Dominique Bachelet and David Turner (Eds.)*
- 214 **Extreme Events: Observations, Modeling and Economics** *Mario Chavez, Michael Chil, and Jaime Urrutia-Fucugauchi (Eds.)*
- 215 **Auroral Dynamics and Space Weather** *Yongliang Zhang and Larry Paxton (Eds.)*
- 216 **Low-Frequency Waves in Space Plasmas** *Andreas Keiling, Dong-Hun Lee, and Valery Nakariakov (Eds.)*
- 217 **Deep Earth: Physics and Chemistry of the Lower Mantle and Core** *Hidenori Terasaki and Rebecca A. Fischer (Eds.)*
- 218 **Integrated Imaging of the Earth: Theory and Applications** *Max Moorkamp, Peter G. Lelievre, Niklas Linde, and Amir Khan (Eds.)*
- 219 **Plate Boundaries and Natural Hazards** *Joao Duarte and Wouter Schellart (Eds.)*
- 220 **Ionospheric Space Weather: Longitude and Hemispheric Dependences and Lower Atmosphere Forcing** *Timothy Fuller-Rowell, Endawoke Yizengaw, Patricia H. Doherty, and Sunanda Basu (Eds.)*
- 221 **Terrestrial Water Cycle and Climate Change Natural and Human-Induced Impacts** *Qihong Tang and Taikan Oki (Eds.)*
- 222 **Magnetosphere-Ionosphere Coupling in the Solar System** *Charles R. Chappell, Robert W. Schunk, Peter M. Banks, James L. Burch, and Richard M. Thorne (Eds.)*
- 223 **Natural Hazard Uncertainty Assessment: Modeling and Decision Support** *Karin Riley, Peter Webley, and Matthew Thompson (Eds.)*
- 224 **Hydrodynamics of Time-Periodic Groundwater Flow: Diffusion Waves in Porous Media** *Joe S. Depner and Todd C. Rasmussen (Auth.)*
- 225 **Active Global Seismology** *Ibrahim Cemen and Yucel Yilmaz (Eds.)*
- 226 **Climate Extremes** *Simon Wang (Ed.)*
- 227 **Fault Zone Dynamic Processes** *Marion Thomas (Ed.)*
- 228 **Flood Damage Survey and Assessment: New Insights from Research and Practice** *Daniela Molinari, Scira Menoni, and Francesco Ballio (Eds.)*
- 229 **Water-Energy-Food Nexus – Principles and Practices** *P. Abdul Salam, Sangam Shrestha, Vishnu Prasad Pandey, and Anil K Anal (Eds.)*
- 230 **Dawn–Dusk Asymmetries in Planetary Plasma Environments** *Stein Haaland, Andrei Rounov, and Colin Forsyth (Eds.)*
- 231 **Bioenergy and Land Use Change** *Zhangcai Qin, Umakant Mishra, and Astley Hastings (Eds.)*
- 232 **Microstructural Geochronology: Planetary Records Down to Atom Scale** *Desmond Moser, Fernando Corfu, James Darling, Steven Reddy, and Kimberly Tait (Eds.)*
- 233 **Global Flood Hazard: Applications in Modeling, Mapping and Forecasting** *Guy Schumann, Paul D. Bates, Giuseppe T. Aronica, and Heiko Apel (Eds.)*
- 234 **Pre-Earthquake Processes: A Multidisciplinary Approach to Earthquake Prediction Studies** *Dimitar Ouzounov, Sergey Pulinet, Katsumi Hattori, and Patrick Taylor (Eds.)*
- 235 **Electric Currents in Geospace and Beyond** *Andreas Keiling, Octav Marghitu, and Michael Wheatland (Eds.)*
- 236 **Quantifying Uncertainty in Subsurface Systems** *Celine Scheidt, Lewis Li, and Jef Caers (Eds.)*
- 237 **Petroleum Engineering** *Moshood Sanni (Ed.)*
- 238 **Geological Carbon Storage: Subsurface Seals and Caprock Integrity** *Stephanie Valle, Jonathan Ajo-Franklin, and J. William Carey (Eds.)*
- 239 **Lithospheric Discontinuities** *Huaiyu Yuan and Barbara Romanowicz (Eds.)*
- 240 **Chemostratigraphy Across Major Chronological Eras** *Alcides N. Sial, Claudio Gaucher, Muthuvairavasamy Ramkumar, and Valderez Pinto Ferreira (Eds.)*
- 241 **Mathematical Geoenergy: Discovery, Depletion, and Renewal** *Paul Pukite, Dennis Coyne, and Daniel Challou (Eds.)*
- 242 **Ore Deposits: Origin, Exploration, and Exploitation** *Sophie Decree and Laurence Robb (Eds.)*
- 243 **Kuroshio Current: Physical, Biogeochemical and Ecosystem Dynamics** *Takeyoshi Nagai, Hiroaki Saito, Koji Suzuki, and Motomitsu Takahashi (Eds.)*
- 244 **Geomagnetically Induced Currents from the Sun to the Power Grid** *Jennifer L. Gannon, Andrei Swidinsky, and Zhonghua Xu (Eds.)*
- 245 **Shale: Subsurface Science and Engineering** *Thomas Dewers, Jason Heath, and Marcelo Sánchez (Eds.)*
- 246 **Submarine Landslides: Subaqueous Mass Transport Deposits From Outcrops to Seismic Profiles** *Kei Ogata, Andrea Festa, and Gian Andrea Pini (Eds.)*
- 247 **Iceland: Tectonics, Volcanics, and Glacial Features** *Tamie J. Jovanelly*
- 248 **Dayside Magnetosphere Interactions** *Qiugang Zong, Philippe Escoubet, David Sibeck, Guan Le, and Hui Zhang (Eds.)*
- 249 **Carbon in Earth's Interior** *Craig E. Manning, Jung-Fu Lin, and Wendy L. Mao (Eds.)*
- 250 **Nitrogen Overload: Environmental Degradation, Ramifications, and Economic Costs** *Brian G. Katz*
- 251 **Biogeochemical Cycles: Ecological Drivers and Environmental Impact** *Katerina Dontsova, Zsuzsanna Balogh-Brunstad, and Gaël Le Roux (Eds.)*
- 252 **Seismoelectric Exploration: Theory, Experiments, and Applications** *Niels Grobbe, André Revil, Zhenya Zhu, and Evert Slob (Eds.)*
- 253 **El Niño Southern Oscillation in a Changing Climate** *Michael J. McPhaden, Agus Santoso, and Wenju Cai (Eds.)*
- 254 **Dynamic Magma Evolution** *Francesco Vetere (Ed.)*
- 255 **Large Igneous Provinces: A Driver of Global Environmental and Biotic Changes** *Richard. E. Ernst, Alexander J. Dickson, and Andrey Bekker (Eds.)*
- 256 **Coastal Ecosystems in Transition: A Comparative Analysis of the Northern Adriatic and Chesapeake Bay** *Thomas C. Malone, Alenka Malej, and Jadran Faganeli (Eds.)*
- 257 **Hydrogeology, Chemical Weathering, and Soil Formation** *Allen Hunt, Markus Egli, and Boris Faybishenko (Eds.)*
- 258 **Solar Physics and Solar Wind** *Nour E. Raouafi and Angelos Vourlidas (Eds.)*
- 259 **Magnetospheres in the Solar System** *Romain Maggiolo, Nicolas André, Hiroshi Hasegawa, and Daniel T. Welling (Eds.)*
- 260 **Ionosphere Dynamics and Applications** *Chaosong Huang and Gang Lu (Eds.)*
- 261 **Upper Atmosphere Dynamics and Energetics** *Wenbin Wang and Yongliang Zhang (Eds.)*
- 262 **Space Weather Effects and Applications** *Anthea J. Coster, Philip J. Erickson, and Louis J. Lanzerotti (Eds.)*
- 263 **Mantle Convection and Surface Expressions** *Hauke Marquardt, Maxim Ballmer, Sanne Cottaar, and Jasper Konter (Eds.)*
- 264 **Crustal Magmatic System Evolution: Anatomy, Architecture, and Physico-Chemical Processes** *Matteo Masotta, Christoph Beier, and Silvio Mollo (Eds.)*
- 265 **Global Drought and Flood: Observation, Modeling, and Prediction** *Huan Wu, Dennis P. Lettenmaier, Qihong Tang, and Philip J Ward (Eds.)*
- 266 **Magma Redox Geochemistry** *Roberto Moretti and Daniel R. Neuville (Eds.)*
- 267 **Wetland Carbon and Environmental Management** *Ken W. Krauss, Zhiliang Zhu, and Camille L. Stagg (Eds.)*
- 268 **Distributed Acoustic Sensing in Geophysics: Methods and Applications** *Yingping Li, Martin Karrenbach, and Jonathan B. Ajo-Franklin (Eds.)*

Geophysical Monograph 268

**Distributed Acoustic Sensing in
Geophysics**
Methods and Applications

**Yingping Li
Martin Karrenbach
Jonathan B. Ajo-Franklin**
Editors

This work is a co-publication of the American Geophysical Union and John Wiley & Sons, Inc.

This edition first published 2022
© 2022 American Geophysical Union

All rights reserved. No part of this publication may be reproduced, stored in a retrieval system, or transmitted in any form or by any means, electronic, mechanical, photocopying, recording, or otherwise, except as permitted by law. Advice on how to obtain permission to reuse material from this title is available at <http://www.wiley.com/go/permissions>.

The rights of Yingping Li, Martin Karrenbach, and Jonathan B. Ajo-Franklin to be identified as the editors of this work have been asserted in accordance with law.

Published under the aegis of the AGU Publications Committee

Matthew Giampoala, Vice President, Publications
Carol Frost, Chair, Publications Committee
For details about the American Geophysical Union visit us at www.agu.org.

Registered Office

John Wiley & Sons, Inc., 111 River Street, Hoboken, NJ 07030, USA

Editorial Office

111 River Street, Hoboken, NJ 07030, USA

For details of our global editorial offices, customer services, and more information about Wiley products, visit us at www.wiley.com.

Wiley also publishes its books in a variety of electronic formats and by print on demand. Some content that appears in standard print versions of this book may not be available in other formats.

Limit of Liability/Disclaimer of Warranty

While the publisher and authors have used their best efforts in preparing this work, they make no representations or warranties with respect to the accuracy or completeness of the contents of this work and specifically disclaim all warranties, including without limitation any implied warranties of merchantability or fitness for a particular purpose. No warranty may be created or extended by sales representatives, written sales materials, or promotional statements for this work. The fact that an organization, website, or product is referred to in this work as a citation and/or potential source of further information does not mean that the publisher and authors endorse the information or services the organization, website, or product may provide or recommendations it may make. This work is sold with the understanding that the publisher is not engaged in rendering professional services. The advice and strategies contained herein may not be suitable for your situation. You should consult with a specialist where appropriate. Further, readers should be aware that websites listed in this work may have changed or disappeared between when this work was written and when it is read. Neither the publisher nor the authors shall be liable for any loss of profit or any other commercial damages, including, but not limited to, special, incidental, consequential, or other damages.

Library of Congress Cataloging-in-Publication Data

Names: Li, Yingping, editor. | Karrenbach, Martin, editor. | Ajo-Franklin, Jonathan, editor.

Title: Distributed acoustic sensing in geophysics : methods and applications / Yingping Li, Martin Karrenbach, Jonathan Ajo-Franklin, editor.

Description: First edition. | Hoboken, NJ : Wiley-American Geophysical Union, [2021] | Series: Geophysical monograph series | Includes bibliographical references.

Identifiers: LCCN 2021015330 (print) | LCCN 2021015331 (ebook) | ISBN 9781119521792 (cloth) | ISBN 9781119521822 (adobe pdf) | ISBN 9781119521778 (epub)

Subjects: LCSH: Geophysics--Methodology. | Optical fiber detectors. | Imaging systems in geophysics. | Microseisms. | Tomography.

Classification: LCC QC808.5 .D57 2021 (print) | LCC QC808.5 (ebook) | DDC 681/.25--dc23

LC record available at <https://lcn.loc.gov/2021015330>

LC ebook record available at <https://lcn.loc.gov/2021015331>

Cover Design: Wiley

Cover Image: © Jonathan Ajo-Franklin

Set in 10/12pt Times New Roman by Straive, Pondicherry, India

CONTENTS

List of Contributors	vii
List of Reviewers	xiii
Preface	xv

Part I Distributed Acoustic Sensing (DAS) Concept, Principle, and Measurements

1 High Definition Seismic and Microseismic Data Acquisition Using Distributed and Engineered Fiber Optic Acoustic Sensors	3
<i>Sergey Shatalin, Tom Parker, and Mahmoud Farhadiroushan</i>	
2 Important Aspects of Acquiring Distributed Acoustic Sensing (DAS) Data for Geoscientists	33
<i>Mark E. Willis, Andreas Ellmauthaler, Xiang Wu, and Michel J. LeBlanc</i>	
3 Distributed Microstructured Optical Fiber (DMOF) Based Ultrahigh Sensitive Distributed Acoustic Sensing (DAS) for Borehole Seismic Surveys	45
<i>Qizhen Sun, Zhijun Yan, Hao Li, Cunzheng Fan, Fan Ai, Wei Zhang, Xiaolei Li, Deming Liu, Fei Li, and Gang Yu</i>	
4 Distributed Acoustic Sensing System Based on Phase-Generated Carrier Demodulation Algorithm.....	57
<i>Tuanwei Xu, Shengwen Feng, Fang Li, Lilong Ma, and Kaiheng Yang</i>	

Part II Distributed Acoustic Sensing (DAS) Applications in Oil and Gas, Geothermal, and Mining Industries

5 Field Trial of Distributed Acoustic Sensing in an Active Room-and-Pillar Mine	67
<i>Xiangfang Zeng, Herbert F. Wang, Neal Lord, Dante Fratta, and Thomas Coleman</i>	
6 On the Surmountable Limitations of Distributed Acoustic Sensing (DAS) Vertical Seismic Profiling (VSP) – Depth Calibration, Directionality, and Noise: Learnings From Field Trials	81
<i>Albena Mateeva, Yuting Duan, Denis Kiyashchenko, and Jorge Lopez</i>	
7 Denoising Analysis and Processing Methods of Distributed Acoustic Sensing (DAS) Vertical Seismic Profiling (VSP) Data.....	93
<i>Yuan-Zhong Chen, Guang-Min Hu, Jun-Jun Wu, Gang Yu, Yan-Peng Li, Jian-Hua Huang, Shi-Ze Wang, and Fei Li</i>	
8 High-Resolution Shallow Structure at Brady Hot Springs Using Ambient Noise Tomography (ANT) on a Trenched Distributed Acoustic Sensing (DAS) Array.....	101
<i>Xiangfang Zeng, Clifford H. Thurber, Herbert F. Wang, Dante Fratta, and Kurt L. Feigl</i>	

Part III Distributed Acoustic Sensing (DAS) Applications in Monitoring of Deformations, Earthquakes, and Microseisms by Fracturing

9 Introduction to Interferometry of Fiber-Optic Strain Measurements	113
<i>Eileen R. Martin, Nathaniel J. Lindsey, Jonathan B. Ajo-Franklin, and Biondo L. Biondi</i>	

10	Using Telecommunication Fiber Infrastructure for Earthquake Monitoring and Near-Surface Characterization	131
	<i>Biondo L. Biondi, Siyuan Yuan, Eileen R. Martin, Fantine Huot, and Robert G. Clapp</i>	
11	Production Distributed Temperature Sensing versus Stimulation Distributed Acoustic Sensing for the Marcellus Shale	149
	<i>Payam Kavousi Ghahfarokhi, Timothy Robert Carr, Cody Wilson, and Keithan Martin</i>	
12	Coalescence Microseismic Mapping for Distributed Acoustic Sensing (DAS) and Geophone Hybrid Array: A Model-Based Feasibility Study	161
	<i>Takashei Mizuno, Joel Le Calvez, and Daniel Raymer</i>	
 Part IV Distributed Acoustic Sensing (DAS) Applications in Environmental and Shallow Geophysics		
13	Continuous Downhole Seismic Monitoring Using Surface Orbital Vibrators and Distributed Acoustic Sensing at the CO2CRC Otway Project: Field Trial for Optimum Configuration	177
	<i>Julia Correa, Roman Pevzner, Barry M. Freifeld, Michelle Robertson, Thomas M. Daley, Todd Wood, Konstantin Tertyshnikov, Sinem Yavuz, and Stanislav Glubokovskikh</i>	
14	Introduction to Distributed Acoustic Sensing (DAS) Applications for Characterization of Near-Surface Processes	191
	<i>Whitney Trainor-Guitton and Thomas Coleman</i>	
15	Surface Wave Imaging Using Distributed Acoustic Sensing Deployed on Dark Fiber: Moving Beyond High-Frequency Noise	197
	<i>Verónica Rodríguez Tribaldos, Jonathan B. Ajo-Franklin, Shan Dou, Nathaniel J. Lindsey, Craig Ulrich, Michelle Robertson, Barry M. Freifeld, Thomas Daley, Inder Monga, and Chris Tracy</i>	
16	Using Distributed Acoustic Sensing (DAS) for Multichannel Analysis of Surface Waves (MASW)	213
	<i>Chelsea E. Lancelle, Jonathan A. Baldwin, Neal Lord, Dante Fratta, Athena Chalari, and Herbert F. Wang</i>	
17	A Literature Review: Distributed Acoustic Sensing (DAS) Geophysical Applications Over the Past 20 Years	229
	<i>Yingping Li, Martin Karrenbach, and Jonathan B. Ajo-Franklin</i>	
Index		293

LIST OF CONTRIBUTORS

Fan Ai

School of Optical and Electronic Information
National Engineering Laboratory for Next Generation
Internet Access System
Huazhong University of Science and Technology
Wuhan, China

Jonathan B. Ajo-Franklin

Department of Earth, Environmental and Planetary
Sciences
Rice University
Houston, Texas, USA
and
Energy Geosciences Division
Lawrence Berkeley National Laboratory
Berkeley, California, USA

Jonathan A. Baldwin

U.S. Army Corps of Engineers
Washington, District of Columbia, USA

Biondo L. Biondi

Department of Geophysics
Stanford University
Stanford, California, USA
and
Institute for Computational and Mathematical
Engineering
Stanford, California, USA

Joel Le Calvez

Schlumberger
Houston, Texas, USA

Timothy Robert Carr

Department of Geology and Geography
West Virginia University
Morgantown, West Virginia, USA

Athena Chalari

Silixa Ltd.
Elstree, UK

Yuan-Zhong Chen

School of Information and Communication Engineering
University of Electronic Science and Technology
of China
Chengdu, China
and
BGP Inc.
China National Petroleum Corporation
Zhuozhou, China

Robert G. Clapp

Department of Geophysics
Stanford University
Stanford, California, USA

Thomas Coleman

Silixa LLC.,
Missoula, Montana, USA

Julia Correa

Energy Geosciences Division
Lawrence Berkeley National Laboratory
Berkeley, California, USA
and
Centre for Exploration Geophysics
Curtin University
Perth, Australia
and
CO2CRC Limited
Melbourne, Australia

Thomas M. Daley

Energy Geosciences Division
Lawrence Berkeley National Laboratory
Berkeley, California, USA

Shan Dou

Visier Inc.
Vancouver, British Columbia, Canada

Yuting Duan

Shell Technology Center
Houston, Texas, USA

Andreas Ellmauthaler

Halliburton
Houston, Texas, USA

Cunzheng Fan

School of Optical and Electronic Information
National Engineering Laboratory for Next Generation
Internet Access System
Huazhong University of Science and Technology
Wuhan, China

Mahmoud Farhadiroushan

Silixa Ltd.
Elstree, UK

Kurt L. Feigl

Department of Geoscience
University of Wisconsin–Madison
Madison, Wisconsin, USA

Shengwen Feng

Key Laboratories of Transducer Technology
Institute of Semiconductors
Chinese Academy of Sciences
Beijing, China
and
College of Materials Science and Opto-Electronic
Technology
University of Chinese Academy of Sciences
Beijing, China

Dante Fratta

Department of Civil and Environmental Engineering
University of Wisconsin–Madison
Madison, Wisconsin, USA

Barry M. Freifeld

Class VI Solutions Inc.
Oakland, California, USA

Stanislav Glubokovskikh

Centre for Exploration Geophysics
Curtin University
Perth, Australia
and
CO2CRC Limited
Melbourne, Australia

Guang-Min Hu

School of Information and Communication Engineering
University of Electronic Science and Technology
of China
Chengdu, China

Jian-Hua Huang

BGP Inc.
China National Petroleum Corporation
Zhuozhou, China

Fantine Huot

Department of Geophysics
Stanford University
Stanford, California, USA

Payam Kavousi Ghahfarokhi

Department of Geology and Geography
West Virginia University
Morgantown, West Virginia, USA

Martin Karrenbach

OptaSense Inc. (A LUNA Company)
Brea, California, USA

Denis Kiyashchenko

Shell Technology Center
Houston, Texas, USA

Chelsea E. Lancelle

Department of Civil and Environmental Engineering
University of Wisconsin–Platteville
Platteville, Wisconsin, USA

Michel J. LeBlanc

Halliburton
Houston, Texas, USA

Fang Li

Key Laboratories of Transducer Technology
Institute of Semiconductors
Chinese Academy of Sciences
Beijing, China
and
College of Materials Science and Opto-Electronic
Technology
University of Chinese Academy of Sciences
Beijing, China

Fei Li

BGP Inc.
China National Petroleum Corporation
Zhuozhou, China

Hao Li

School of Optical and Electronic Information
National Engineering Laboratory for Next Generation
Internet Access System
Huazhong University of Science and Technology
Wuhan, China

Xiaolei Li

OVLINK Inc.
Wuhan, China

Yan-Peng Li

BGP Inc.
China National Petroleum Corporation
Zhuozhou, China

Yingping Li

BlueSkyDas (formerly Shell)
Houston, Texas, USA

Nathaniel J. Lindsey

FiberSense
Sydney, Australia

Deming Liu

School of Optical and Electronic Information
National Engineering Laboratory for Next Generation
Internet Access System
Huazhong University of Science and Technology
Wuhan, China

Jorge Lopez

Shell Brasil Petróleo Ltda.
Rio de Janeiro, Brazil

Neal Lord

Department of Geoscience
University of Wisconsin–Madison
Madison, Wisconsin, USA

Lilong Ma

Key Laboratories of Transducer Technology
Institute of Semiconductors
Chinese Academy of Sciences
Beijing, China
and
College of Materials Science and Opto-Electronic
Technology
University of Chinese Academy of Sciences
Beijing, China

Eileen R. Martin

Department of Mathematics
Virginia Polytechnic Institute and State University
Blacksburg, Virginia, USA

Keithan Martin

Department of Geology and Geography
West Virginia University
Morgantown, West Virginia, USA

Albena Mateeva

Shell Technology Center
Houston, Texas, USA

Takashi Mizuno

Schlumberger
Houston, Texas, USA

Inder Monga

Energy Sciences Network
Lawrence Berkeley National Laboratory
Berkeley, California, USA

Tom Parker

Silixa Ltd.
Elstree, UK

Roman Pevzner

Centre for Exploration Geophysics
Curtin University
Perth, Australia
and
CO2CRC Limited
Melbourne, Australia

Daniel Raymer

Schlumberger
Houston, Texas, USA

Michelle Robertson

Energy Geosciences Division
Lawrence Berkeley National Laboratory
Berkeley, California, USA

Verónica Rodríguez Tribaldos

Energy Geosciences Division
Lawrence Berkeley National Laboratory
Berkeley, California, USA

Sergey Shatalin

Silixa Ltd.
Elstree, UK

Qizhen Sun

School of Optical and Electronic Information
National Engineering Laboratory for Next Generation
Internet Access System
Huazhong University of Science and Technology
Wuhan, China

Konstantin Tertyshnikov

Centre for Exploration Geophysics
Curtin University
Perth, Australia
and
CO2CRC Limited
Melbourne, Australia

Clifford H. Thurber

Department of Geoscience
University of Wisconsin–Madison
Madison, Wisconsin, USA

Chris Tracy

Energy Sciences Network
Lawrence Berkeley National Laboratory
Berkeley, California, USA

Whitney Trainor-Guitton

Department of Geophysics
Colorado School of Mines
Golden, Colorado, USA
and
W Team Geosolutions
Twin Falls, Idaho, USA

Craig Ulrich

Energy Geosciences Division
Lawrence Berkeley National Laboratory
Berkeley, California, USA

Herbert F. Wang

Department of Geoscience
University of Wisconsin–Madison
Madison, Wisconsin, USA

Shi-Ze Wang

BGP Inc.
China National Petroleum Corporation
Zhuozhou, China

Mark E. Willis

Halliburton
Houston, Texas, USA

Cody Wilson

Department of Geology and Geography
West Virginia University
Morgantown, West Virginia, USA

Todd Wood

Energy Geosciences Division
Lawrence Berkeley National Laboratory
Berkeley, California, USA

Jun-Jun Wu

BGP Inc.
China National Petroleum Corporation
Zhuozhou, China

Xiang Wu

Halliburton Far East Pte. Ltd.
Singapore

Tuanwei Xu

Key Laboratories of Transducer Technology
Institute of Semiconductors
Chinese Academy of Sciences
Beijing, China
and
College of Materials Science and Opto-Electronic
Technology
University of Chinese Academy of Sciences
Beijing, China

Zhijun Yan

School of Optical and Electronic Information
National Engineering Laboratory for Next Generation
Internet Access System
Huazhong University of Science and Technology
Wuhan, China

Kaiheng Yang

Key Laboratories of Transducer Technology
Institute of Semiconductors
Chinese Academy of Sciences
Beijing, China
and
College of Materials Science and Opto-Electronic
Technology
University of Chinese Academy of Sciences
Beijing, China

Sinem Yavuz

Centre for Exploration Geophysics
Curtin University
Perth, Australia
and
CO2CRC Limited
Melbourne, Australia

Gang Yu

BGP Inc.
China National Petroleum Corporation
Zhuozhou, China
and
School of Information and Communication Engineering
University of Electronic Science and Technology
of China
Chengdu, China

Siyuan Yuan

Department of Geophysics
Stanford University
Stanford, California, USA

Xiangfang Zeng

State Key Laboratory of Geodesy and Earth's
Dynamics

Innovation Academy for Precision
Measurement Science and Technology
Chinese Academy of Sciences
Wuhan, China

and

Department of Geoscience
University of Wisconsin–Madison
Madison, Wisconsin, USA

Wei Zhang

School of Optical and Electronic Information
National Engineering Laboratory for Next Generation
Internet Access System
Huazhong University of Science and Technology
Wuhan, China

LIST OF REVIEWERS

Reza Barati
Matt Becker
Gary Binder
Biondo L. Biondi
Stefan Buske
Dongjie Cheng
Feng Cheng
Steve Cole
Julia Correa
Thomas M. Daley
Timothy Dean
Yuting Duan
Mahmoud Farhadiroushan
Barry M. Freifeld
Andrew Greenwood
Alireza Haghighat
Ge Jin
John Michael Kendall
Hunter Knox
Ivan Lim Chen Ning
Nathaniel J. Lindsey
Min Lou
Linqing Luo
Stefan Lüth
Eileen R. Martin
Robert Mellors
Khalid Miah

Douglas Miller
Takashi Mizuno
Gerrit Olivier
Roman Pevzner
Michelle Robertson
Verónica Rodríguez Tribaldos
Bill Roggenthen
Baishali Roy
Ali Sayed
Alireza Shahkarami
Robert Stewart
Aleksei Titov
Whitney Trainor-Guitton
Milovan Urosevic
Guchang Wang
Herbert F. Wang
Erik Westman
Ethan Williams
Mark E. Willis
Xiangfang Zeng
Ge Zhan
Zhongwen Zhan
Haijiang Zhang
Ran Zhou
Ding Zhu
Tieyuan Zhu

PREFACE

Distributed acoustic sensing (DAS) systems are optoelectronic instruments that measure acoustic interactions (distributed strain or strain rate) along the length of a fiber-optic sensing cable. DAS observation systems can record sound and vibration signals along several tens of kilometers of sensing optical fiber with fine spatial resolution (1–10 m) and over a wide frequency range (from millihertz to tens of kilohertz). DAS provides a large sensing aperture for acquiring high-resolution acoustic data in both time and space domains. The advantages of DAS technology have enabled its rapid adoption across a range of applications, including geophysics, geohydrology, environmental monitoring, geotechnical and civil engineering (railroad, tunnel, and bridge monitoring), hazard mitigation and prevention, and safety and security fields.

This monograph focuses on various DAS applications in geophysics. The use of DAS in the oil, gas, geothermal, and mining industries for high-resolution borehole and surface seismic imaging, and microseismic monitoring for hydraulic fractures has accelerated with improvements in the sensitivity of DAS instruments, advances in real-time big data processing, and flexible and economic deployment of fiber-optic sensing cables. There is also growing interest in using DAS for critical geophysical infrastructure applications, such as earthquake and near-surface passive seismic analysis, including the development of tailored or novel numerical techniques. This book aims to engage both the scientific and industrial communities to share their knowledge and experiences of using DAS for novel geophysical applications.

The origin of this book was the 2017 American Geophysical Union (AGU) Fall Meeting, when scientists and engineers from both industry and academia gathered in New Orleans to present their fantastic research outcomes on DAS instrumentations and applications in geophysics and seismology. As DAS technologies have continued to advance, more and more successful geophysical DAS applications have been reported and published in different geophysical and seismological journals, abstracts, and proceedings of technical conferences, such as the AGU, the Society of Exploration Geophysicists (SEG), the European Association of Geoscientists and Engineers (EAGE), the Society of Petroleum Engineers (SPE), and the Seismological Society of America (SSA). However, few DAS books are available on DAS principles, instrumentation, and geophysical applications. Many attendees at the DAS sessions at the 2017 AGU Fall Meeting expressed that there was a

need for a book on DAS geophysical applications. We had interesting discussions with many scientists and engineers working on the frontier of DAS geophysical applications about the potential for a book. We specially recognize Biondo L. Biondi, Thomas M. Daley, William Ellsworth, Mahmoud Farhadiroushan, Barry M. Freifeld, Albena Mateeva, Robert Mellors, Clifford H. Thurber, Herbert Wang, and Mark E. Willis, as well as many others for their encouragement.

During the 2017 AGU Fall Meeting in New Orleans, we fortunately got an opportunity to meet with the AGU Books Editor, Dr. Bose, who was already aware of this rapidly growing scientific field. We discussed a potential book on DAS geophysical applications, and she was very supportive and invited us to submit a book proposal for an AGU monograph. With no surprise, this DAS book proposal received very positive comments and constructive suggestions from all reviewers. Several reviewers also asked for an opportunity to submit their own contributions to this monograph. We are grateful to those anonymous reviewers of the book proposal for their positive comments and constructive suggestions that led this book to be initiated.

This monograph is organized into four parts. Part I starts with principles of DAS measurements and instruments. DAS interrogation units transmit a pulse of laser light into the fiber. As this pulse of light travels down the fiber, interactions within the fiber result in light reflections known as backscatter (Rayleigh scattering). Backscatters are determined by tiny strain events within the fiber, which in turn are caused by localized acoustic energy. This backscattered light travels back up the fiber toward the interrogation unit where it is sampled. Part II introduces various DAS applications in the oil and gas, geothermal, and mining industries. Part III looks at DAS applications in seismic monitoring. DAS microseismic monitoring of hydraulic fracturing is an industry application but with passive seismic sources. The microseismic DAS method has been shown to have sufficient sensitivity to record very small magnitude microearthquakes with DAS deployed in boreholes. Microseismic DAS systems can be naturally extended to monitoring larger earthquake activity, and slow deformation of Earth's structure with large-scale fiber-optic networks. Part IV discusses DAS environmental and shallow geophysical applications such as geological carbon dioxide sequestration. The final chapter presents a review of fiber optical sensing applications in geophysics including historical

developments and recent advances. The list of over 900 literature references of DAS and related technologies will benefit readers, especially newcomers who have just stepped into this fast-growing field.

We would like to thank the AGU Books Editorial Board for supporting this monograph. Without the efforts from contributing authors it would not have been possible to accomplish this project. We would also like to thank the many volunteer reviewers who spent tremendous amounts of time and effort to ensure that each chapter is of the highest quality. We appreciate Jonathan B. Ajo-Franklin, Biondo L. Biondi, Mahmoud Farhadiroushan, Albena Mateeva, and Siyuan Yuan for providing their pictures as candidates for the book cover design. Thanks are also extended to the AGU Books editorial team at Wiley, especially Dr. Rituparna Bose, Layla Harden, Noel McGlinchey, Vaishali Rajasekar, Sangaprabha Mohan, Bobby Kilshaw, Nithya Sechin, and Emily Bae, for their organization, management, and cover design.

This monograph will be the first comprehensive handbook for anyone interested in learning DAS principles and applications. We hope that the book will have a wide spectrum of readers – such as geophysicists, seismologists, geologists, and geoscientists; environmental scientists; and graduate and undergraduate students in geophysics and geoscience – with a common interest in DAS geophysical applications. This book also provides a common platform to the scientific and industry communities to share state-of-the-art DAS technology.

Yingping Li

BlueSkyDas (formerly Shell), USA

Martin Karrenbach

OptaSense Inc. (A LUNA Company), USA

Jonathan B. Ajo-Franklin

*Rice University and Lawrence Berkeley
National Laboratory, USA*

Part I

Distributed Acoustic Sensing (DAS) Concept, Principle, and Measurements

High Definition Seismic and Microseismic Data Acquisition Using Distributed and Engineered Fiber Optic Acoustic Sensors

Sergey Shatalin, Tom Parker, and Mahmoud Farhadiroushan

ABSTRACT

The distributed acoustic sensor (DAS) offers a new versatile tool for geophysical applications. The system allows seismic signals to be recorded along tens of kilometers of optical fiber and over a wide frequency range. In this chapter we introduce the concept of DAS and derive an expression for the system response by modeling the superposition of the coherent backscatter fields along the fiber. Expressions are derived for converting the optical phase to strain rate and equivalent particle motion. We discuss DAS signal processing and denoising methods to deal with the random nature of the Rayleigh scatter signal and to further improve dynamic range and sensitivity. Next we consider DAS parameters such as spatial resolution, gauge length and directionality in comparison with geophones. We present some field trial results that demonstrate the benefits of the DAS for vertical seismic profiling and microseismic detection. Finally we discuss the fundamental sensitivity limit of DAS. We consider how the scattering properties of conventional fiber can be engineered to deliver a step-change DAS performance, beyond that of conventional geophones and seismometers. Theoretical findings are illustrated by the field data examples, including low-frequency strain monitoring and microseismic detection.

1.1. DISTRIBUTED ACOUSTIC SENSOR (DAS) PRINCIPLES AND MEASUREMENTS

In this chapter, we consider the principles and performance of distributed and precision engineered fiber optic acoustic sensors for geophysical applications (Hartog et al., 2013; Parker et al., 2014). In particular, system parameters such as spatial resolution, dynamic range, sensitivity, and directionality are examined for seismic and microseismic measurements.

In this first section, we consider the measurement principle of DAS, which uses naturally occurring

random scatter centers along the fiber. We use the term *acoustics* in a broad physical sense here, like any propagation of mechanical disturbances (Lewis, 1985). We review different DAS systems, including direct-intensity-detection and phase-detection schemes, where we derive a mathematical relationship for optical phase recovery. Our aim is to explain the nature of the distributed acoustic signal and describe the natural limitations for DAS measurements. Such information is needed to optimize DAS recording parameters for geophysical applications. Examples of DAS parameter optimization for seismic applications can be found in Section 1.2. We also present some examples of active and passive seismic field data in Sections 1.2 and 1.3.

Silixa Ltd. Elstree, UK

Distributed Acoustic Sensing in Geophysics: Methods and Applications, Geophysical Monograph 268, First Edition.

Edited by Yingping Li, Martin Karrenbach, and Jonathan B. Ajo-Franklin.

© 2022 American Geophysical Union. Published 2022 by John Wiley & Sons, Inc.

DOI:10.1002/9781119521808.ch01

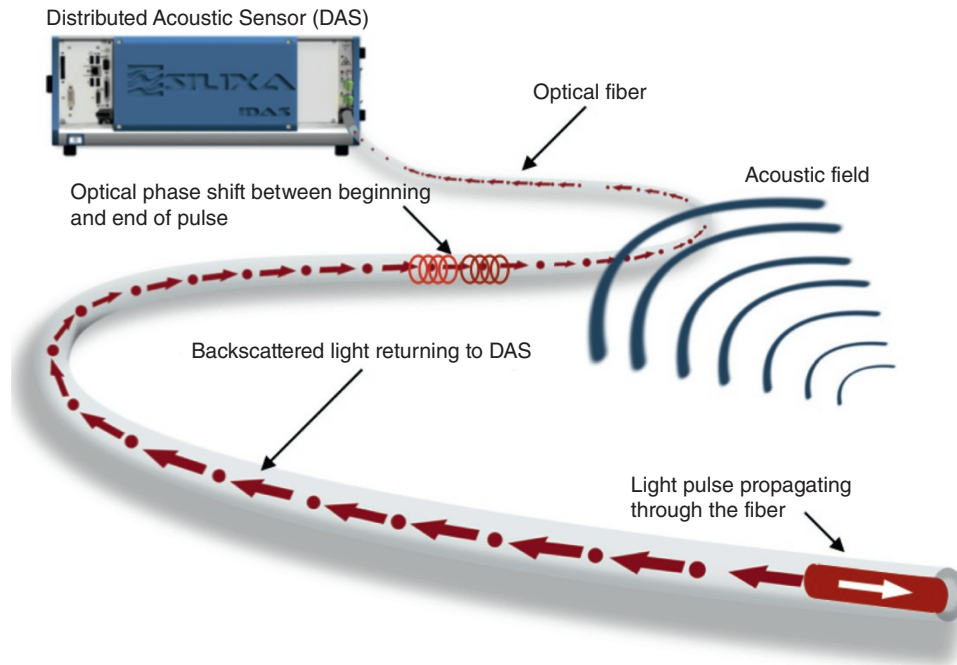


Figure 1.1 Operation principle of distributed acoustic sensing.

1.1.1. DAS Concept

The principle of distributed sensing is based on *optical time domain reflectometry* (OTDR), as indicated in Figure 1.1. When a laser pulse travels down an optical fiber, a tiny portion of the light is naturally scattered through Rayleigh, Raman (Dakin & Culshaw, 1989), and Brillouin (Parker et al., 1998) interactions and returns to the optoelectronic sensor unit. The measurement location can be determined from the time taken for the laser pulse to travel down the sensing fiber, and the backscatter light to return to the optoelectronic sensor unit.

Figure 1.1 shows the basic principle of DAS, where the sensing fiber is excited with a coherent laser pulse and the Rayleigh backscattered interference along the fiber is detected and digitized. An acoustic wave elongates the fiber and so changes the optical phase shift between backscatter components from the leading and trailing parts of the optical pulse. As a result of interference, the intensity of the returning light changes from pulse to pulse. It is also possible to determine the optical phase to recover acoustic phase so there are two classes of DAS, based on the detection of: (i) optical intensity and (ii) optical phase. With the intensity DAS technique, also referred to as *coherent optical time domain reflectometry* (COTDR), a perturbation along the fiber is detected by measuring the changes in the backscatter intensity from pulse to pulse, as indicated in Figure 1.2. COTDR has been used for the detection of temperature changes (Rathod et al., 1994; Shatalin et al., 1991) and acoustic vibration (Juškaitis et al., 1992; Posey

et al., 2000), along multi-kilometer fiber cables (Juarez et al., 2005; Shatalin et al., 1998).

The principle of the COTDR system can be understood by analyzing the radiation generated by localized scatter centers (Taylor & Lee, 1993). Here, the coherent scattered light can be represented as the result of two reflections with random amplitude and phase. When the fiber is strained, the backscatter intensity varies in accordance with the strain rate (Figure 1.2), but with an unpredictable amplitude and phase, which changes along the fiber (Shatalin et al., 1998). As a result, the signal cannot be effectively accumulated for multiple seismic pulses: the fiber response to strain is highly nonlinear, and therefore the changes in amplitude and phase cannot be directly matched to the original strain affecting the fiber. The next section discusses ways of addressing this. Therefore, COTDR systems are not that useful for seismic applications.

With the phase DAS technique, the method for optical phase analysis is a key feature of system design. All techniques rely on phase modulation between the beginning and end of a pulse, which can be considered as a double pulse. Such modulation can be performed before or after light propagation over optical fiber, as indicated in Figure 1.3. We have limited our discussion to schemas that have been patented and implemented in practice. In one scheme, which is similar to that used for multiplexed interferometer sensors (Dakin, 1990), two laser pulses with different frequencies may be sent down the fiber (Figure 1.3a). In this case, the acoustic phase shift

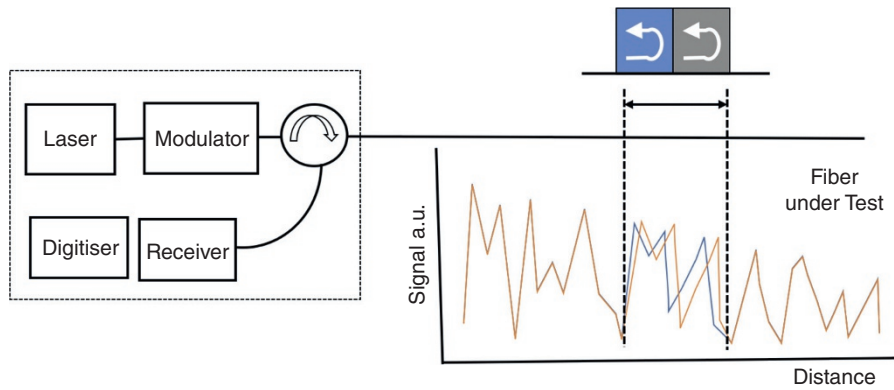


Figure 1.2 COTDR.

Method	Adapted schematic diagram	Reference
a Two pulses with shifted frequencies and embedded delay		Crickmore & Hill, 2010
b Interferometer with 3x3 coupler and embedded delay		Farhadiroushan et al., 2010
c Heterodyne		Hartog & Kader 2012
d Different frequency comparator		Farhadiroushan et al., 2010 Handerek, 2016 Crickmore & Ku, 2017

Figure 1.3 DAS schemas: MOD—intensity and frequency modulator; AOM—acousto-optic modulator.

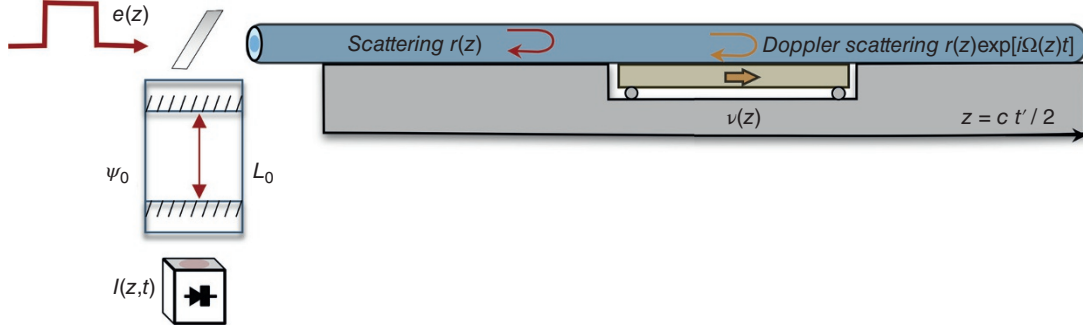


Figure 1.4 DAS optical setup. Distance is proportional to flytime.

will be transferred to a frequency difference and can be measured in the photocurrent radio frequency domain.

Other solutions, such as that shown in Figure 1.3b, contain an embedded delay line that defines the spatial resolution. We will focus our analysis on this class of systems. Another configuration uses optical heterodyne, as shown in Figure 1.3c, where the backscatter signal is continuously mixed with a slightly frequency shifted local oscillator laser. In this case, the elongation along the fiber is measured by computing the difference of the accumulated optical phase between two sections of fiber, and the measurement is carried out at differential frequency $f_1 - f_2$. Although this technique offers a flexible spatial resolution, it requires a laser source with extremely high coherence to achieve reasonable signal-to-noise ratio (SNR) performance over several tens of kilometers of fiber. The details of the heterodyne concept are thoroughly covered elsewhere (Hartog, 2017). Another method involves sending multiple pulses of different frequencies, either in series or from pulse to pulse, and then computing the phase of the backscatter signal, as indicated in Figure 1.3d. The phase calculation in this case is similar to first case (Figure 1.3a).

1.1.2. DAS Interferometric Optical Response

The theoretical concept of DAS is based on the assumption that the Rayleigh centers have no microscopic motion, but they are “frozen” inside glass during manufacture. In this case, the positions of the centers depend on the macroscopic motion of fiber and can coincide with the ground speed around a buried fiber (v). There are two time scales of relevance to DAS: (1) as optical pulse travels with speed c , significantly faster than ground motion, this dictates the spatial resolution; (2) seismic motion is responsible for interference changes pulse to pulse, which can be used to recover the seismic signal. All parameters for both fast and slow motions are summarized in the table of variables at the end of the chapter.

Let us calculate how the intensity of backscattered light changes when a section of fiber is moving with speed $v(z)$ under a seismic wave (Figure 1.4). The Rayleigh centers will move with the fiber, so the frequency of the backscattered light will experience a Doppler shift $\Omega(z)$ proportional to its speed, like for Brillouin scattering (Hartog, 2017). The aim of DAS can be considered as the measurement of Doppler shift for Rayleigh scattering derived from the detected photocurrent. The phase shift can be measured between two separate points in space, and then the resultant Doppler shift can be recovered with spatial integration, as will be shown later in the text. The first step is to analyze changes in intensity between different optical pulses to derive the fiber speed information, which will be equal to the ground speed in a seismic wave.

Consider a coherent optical pulse $e(t')$ that is launched into a single-mode optical fiber. The backscattered optical field $E(t')$ at time t' for light reemerging from the launch end can be expressed as a superimposition of delayed partial fields backscattered with a reflection coefficient $r_0(z)$ along the fiber axis z (Shatalin et al., 1998). This amplitude coefficient represents coupling between the forward and backward modes. For a speed of light in the fiber $c \approx 2 \cdot 10^8 \text{ m/c}$, and wave propagation constant β , we can use group and phase delays $2z/c$ and $2 \int_0^z \beta(x) dx$, respectively. So, the emerging field will depend on interferometer optical delay, or gauge length, L_0 as:

$$E(t') = \int_0^{L_0} \left[e\left(t' - \frac{2z}{c}\right) + e\left(t' - \frac{2z}{c} - \frac{2L_0}{c}\right) \right] \cdot r_0(z) \cdot \exp\left[2i \int_0^z \beta(x) dx\right] dz \quad (1.1)$$

For a regular fiber, the phase shift term in Equation 1.1 can be separated into a constant part and a part changing with “slow” time t , representing pulse-to-pulse parameter

variation with Doppler shift frequency $\Omega(z)$, which is proportional to scattering particle velocity $v(z)$ and wavelength frequency ω .

$$\int_0^z \beta(x, t) dx = \beta_0 z + \Omega(z)t \quad (1.2)$$

$$\Omega(z) = \omega v(z)/c = \frac{4\pi n_{eff} K_\epsilon}{\lambda} v(z) \quad (1.3)$$

Here the strain coefficient K_ϵ relates the physical and optical length of fiber, n_{eff} is fiber effective refractive index, and λ is the laser wavelength. Equations 1.2–1.3 represent a well-known dualism, when a change in interference can be considered not only as a result of a change in phase, but also as a beating of a frequency due to a Doppler shift. The concept finds application in Doppler lidars, where Rayleigh scattering light contains wind speed information, so the height distribution of the speed can be detected using OTDR (Garnier & Chanin, 1992). The DAS conception is somewhat different: we do not measure the absolute velocity of Rayleigh scatterers, but the difference in such velocity along the gauge length. Another difference is that Rayleigh centers are frozen in a glass of fiber at a melting point of about 800°. Their movement follows the movement of the fiber, and hence very low Doppler frequencies (down to mHz) can be measured.

For simplicity of further calculations, the reflective coefficient $r_0(z)$ can be redefined as the effective reflective coefficient $r(z)$:

$$r(z) = r_0(z) \exp(\beta_0 z) \quad (1.4)$$

Then, to extract the Doppler shift from the intensity equation, we need to control the phase shift ψ_0 between delayed optical fields in the interferometer. So Equation 1.1 can be rearranged using Equations 1.2–1.4 to:

$$E(z, t) = [e(z) + e(z - L_0) \cdot \exp i\psi_0] \otimes r(z) \exp i[\Omega(z)t] \quad (1.5)$$

Here the convolution symbol \otimes is used to simplify the expression, and the OTDR scale $z = 2ct'$ for the “fast” time t' is used. The convolution commutes with translations (Goodman, 2005), meaning that Equation 1.5 can be converted using $a(z_1 - z_2) \otimes b(z_1) = a(z_1) \otimes b(z_1 - z_2)$ to:

$$E(z, t) = e(z) \otimes \{r(z) \exp i[\Omega(z)t] + r(z - L_0) \exp i[\Omega(z - L_0)t + \psi_0]\} \quad (1.6)$$

Let us consider first the simple case of short pulse $e(z) = \delta(z)$ when δ is the Dirac delta function. Then convolution can be removed from Equation 1.5 because $\delta(z) \otimes a(z) = a(z)$, and the distance variation of Doppler

shift $\Delta\Omega(z) = \Omega(z) - \Omega(z - L_0)$ can be represented via variation of intensity $I(z, t) = E(z, t)E(z, t)^*$. The expression in braces in Equation 1.6 represents a two-beam interference, so the intensity will vary harmonically depending on the phase. As we are interested in the intensity change, only the interference term needs be taken into consideration, which can be reshaped using the intensity derivative:

$$\frac{\partial I}{\partial t} = \frac{\partial E(z, t)}{\partial t} E(z, t)^* + E(z, t) \frac{\partial E(z, t)^*}{\partial t} \quad (1.7)$$

Then using convolution properties $\partial[a \otimes b(t)]/\partial t = a \otimes \partial b(t)/\partial t$, we can find intensity variation via phase shift Φ of backscattered light where there is argument of backscattering complex function:

$$\frac{\partial I}{\partial t} = 2\Delta\Omega(z) |r(z)r(z - L_0)^*| \sin(\psi_0 + \Phi) \quad (1.8)$$

$$\Phi = \Delta\Omega(z)t + \text{Arg}[r(z)r(z - L_0)^*] \quad (1.9)$$

The COTDR signal can be deduced from Equation 1.8 if we set $L_0 = 0$ and $\psi_0 = 0$. Even such a simple setup can deliver information on the Doppler shift and hence the ground speed $v(z)$ through the intensity variation $\partial I/\partial t \propto \Delta v$ in accordance with Equations 1.3, 1.8. Unfortunately, the proportionality factor contains an oscillation term, so we cannot distinguish positive speed from negative.

The result of computer modeling of a COTDR response on a differential Ricker wavelet for ground speed (Hartog, 2017) is presented in Figure 1.5. The right side shows 1D seismic wave moving in the z direction (in m) with a reflection from an interface with a positive reflection coefficient. Below the image is a time series of apparent velocity, when units are normalized to the expected optical phase shift in radians between points separated by gauge length 10 m. The left side of the figure corresponds to the relative pulse-to-pulse variation of the COTDR signal calculated in accordance with Equations 1.8–1.9. The sign of response changes randomly in accordance with an optical pulsewidth of 50 ns or 5 m. As a result, the signal cannot be effectively accumulated for multiple seismic pulses because of the temperature drift between seismic shots. Temperature drift changes the phase constant of the fiber β_0 and, in accordance with Equation 1.4, the effective reflection coefficient $r(z)$ also changes. As a result of such drift, every seismic shot will have a unique, random, alternating, speckle-like signature that cancels the averaging sum. Fortunately, this problem can be overcome by optical phase recovery, when, after similar averaging, average values appear. Thus, the actual DAS output will be a combination of fiber speed information and the unaveraged portion of the random COTDR signal.

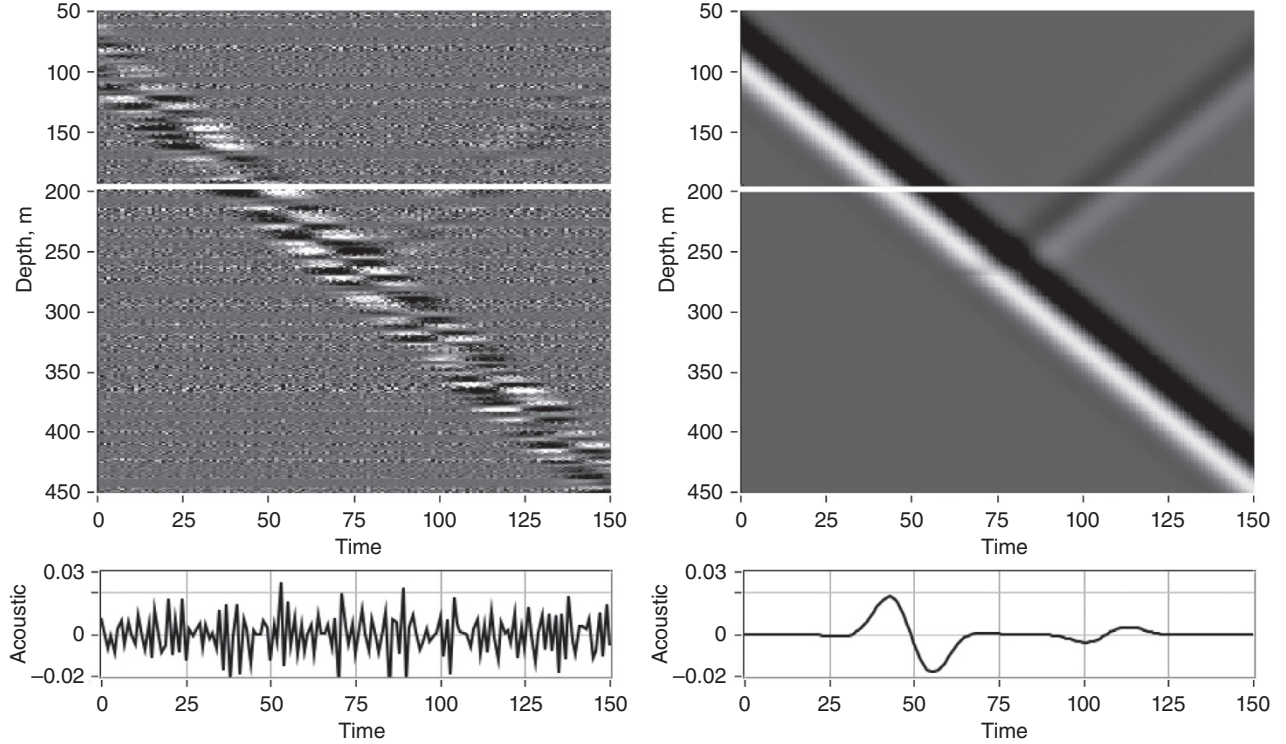


Figure 1.5 COTDR response (Equation 1.6) shown in the left panel of the simulated signal of a ground velocity wavelet shown in the right panel. The signals' cross-section along the white line is shown in the bottom panels in radians. Source: Based on Correa et al. (2017).

1.1.3. DAS Optical Phase Recovery

The randomness of the COTDR signal can be reduced through proper control of the external interferometer phase shift ψ_0 , which can be achieved in many ways. All these methods are based on the fact that COTDR intensity is random in distance but will vary harmonically depending on the phase, as follows from Equation 1.1 (see Figure 1.6). So, phase control can reveal phase information regardless of the random nature of the signal.

We will start our phase analysis with a simple, although not very practical, approach, where the phase shift ψ_0 is locked onto a fringe $\sin(\psi_0 + \Phi) \equiv 1$. Such an approach was used earlier to analyze the spatial resolution in phase microscopy (Rea et al., 1996). Then Equations 1.8 and 1.9 can be averaged over an ensemble of delta correlated backscattering coefficients $\langle r(u)r(w) \rangle = \rho^2 \delta(u - w)$ as:

$$\left\langle \frac{\partial I(z, t)}{\partial t} \right\rangle = 2\rho^2 \Delta\Omega(z) \quad (1.10)$$

$$\left\langle \frac{\partial \Phi(z, t)}{\partial t} \right\rangle = \frac{1}{2\rho^2} \left\langle \frac{\partial I(z, t)}{\partial t} \right\rangle \quad (1.11)$$

Equation 1.10 demonstrates that the sign of Doppler shift can be measured by DAS with proper phase control.

The same data can be extracted directly from phase information, as is clear from Equation 1.11.

So far, we have analyzed the short pulse case, where the pulsewidth is significantly smaller than the external interferometer delay. In reality, such pulses cannot deliver significant optical power, which is necessary for precise measurements. Fortunately, Equations 1.10–1.11 can be generalized for a nonzero length optical pulse $e(z)$ directly from Equation 1.5 in the same way that an optical incoherent image was obtained in Goodman (2005) using correlation averaging $\langle (a \otimes r_1)(a \otimes r_2) \rangle = \langle a^2 \rangle \otimes \langle r_1 r_2 \rangle$. This expression is valid for an uncorrelated field, generated by random reflection points $\langle r_1(z_1)r_2(z_2) \rangle = \delta(z_1 - z_2)$. This calculation confirms that Equation 1.11 remains the same, as it represents averaging over different harmonic signals, but Equation 1.10 will be reshaped to:

$$\left\langle \frac{\partial I(z, t)}{\partial t} \right\rangle = 2\rho^2 e(z)^2 \otimes \Delta\Omega(z) \quad (1.12)$$

Equation 1.11 gives us the possibility to introduce a dimensionless signal as a phase change over a repetition or sampling frequency F_S period $A(z) = F_S \cdot \partial\Phi/\partial t$, and so the DAS output $A(z)$ can be represented for pulsewidth $\tau(z) = e(z)^2$ from Equations 1.3, 1.10, and 1.11 as:

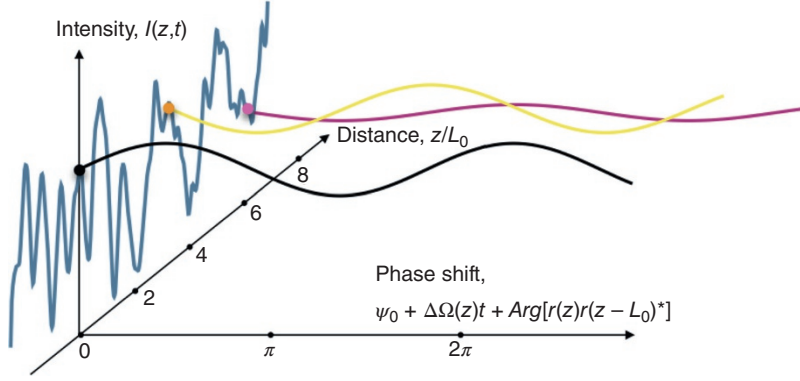


Figure 1.6 Intensity changes are irregular along distance but harmonic along phase shift axis.

$$\langle A(z) \rangle = \frac{1}{A_0 F_S} \cdot \tau(z) \otimes [v(z) - v(z - L_0)] \quad (1.13)$$

$$A_0 = \frac{\lambda}{4\pi n_{eff} K_e} = 115nm \quad (1.14)$$

In Equation 1.14, the elongation corresponding to $\Delta\Phi = 1 \text{ rad}$ is $A_0 = 115nm$, calculated for $\lambda = 1550$, $n_{eff} = 1.468$ and $K_e = 0.73$, which has been measured for conventional fiber (Kreger et al., 2006). The DAS signal is a convolution of pulse shape (as is typical for OTDR-type distributed sensors) with a measured field, which is the spatial difference in fiber elongation speed of points separated by a gauge length.

Phase measurements can be made in a more practical way than locking the interferometer onto a fringe by using intensity trace $I_j(z, t)$ $j = 1, 2, \dots, P$ from P multiple interferometers with different phase shifts. Such data can be collected consequentially in P optical pulses, but it reduces sensor bandwidth by P times. Alternatively, the information can be collected for one pulse using a multi-output optical component, such as a 3×3 coupler. In the general case, the phase shift $\Phi(z, t)$ can be represented (Todd, 2011) via the arctangent function ATAN of the ratio of imaginary $\text{Im } Z$ to real part $\text{Re } Z$ of linear combinations of intensities:

$$\Phi(z, t) = \text{ATAN} \left(\frac{\text{Im } Z}{\text{Re } Z} \right) = \text{ATAN} \frac{\sum_{j=1}^P \alpha_j I_j(z, t)}{\sum_{j=1}^P \gamma_j I_j(z, t)} \quad (1.15)$$

$$V = \sqrt{\text{Im } Z^2 + \text{Re } Z^2} \quad (1.16)$$

where V is the visibility given by the ratio of peak-to-peak intensity variation to average intensity of the interference signal. In particular, for a symmetrical 3×3 coupler,

$\text{Im } Z = \sqrt{3}I_1 - \sqrt{3}I_3$ and $\text{Re } Z = I_1 - 2I_2 + I_3$. An additional modification of Equation 1.15 including phase unwrapping will be discussed in the next section. It is interesting to mention that a heterodyne approach (Hartog et al., 2013) can also use quadrature measurements similar to Equation 1.15, but in that case phase diversity is realized in the OTDR time/distance scale, which can affect spatial resolution. Also, we can mention that the interferometer approach does not need a highly coherent laser, as the optical lengths of interfering rays are nearly compensated (Posey et al., 2000).

The theoretical expression for DAS resolution (Equation 1.13) was obtained from analysis of an interferometer locked onto a fringe, and it is necessary to test how this is applicable to practical phase measurement algorithms. Also, Equation 1.13 contains averaging over a statistical ensemble, and it is important to understand what it means in a real application. To answer the questions, we have compared theoretical values with a simulation based on a 3×3 coupler setup for 100 different random Rayleigh scattering patterns for a wide variety of parameters and found good comparison after averaging. To illustrate this analysis, three optical pulsewidth settings were used for interferometer delay (gauge length) of $L_0 = 10m$ and a ground velocity zone of 40 m (Figure 1.7a–c).

All traces (Figure 1.7a–c) correspond to strain measurements rather than to ground velocity profile measurements. If the pulsewidth is small, $\tau = 10ns$, then averaging is not important, and the correspondence between different phase recovery algorithms are clear (Figure 1.7a). For a reasonable pulsewidth, $\tau = 50ns$, only averaged simulation results correspond to theory (Figure 1.7b). If pulsewidth $\tau = 100ns$ becomes equal to $L_0 = 10m$ in the OTDR scale, then averaging is critical, but after it 100 times averaging correspondence is good (Figure 1.7c). It is important to mention that this simulation did not include photodetector noise, and noise-like performance in Figure 1.7c can be explained by the

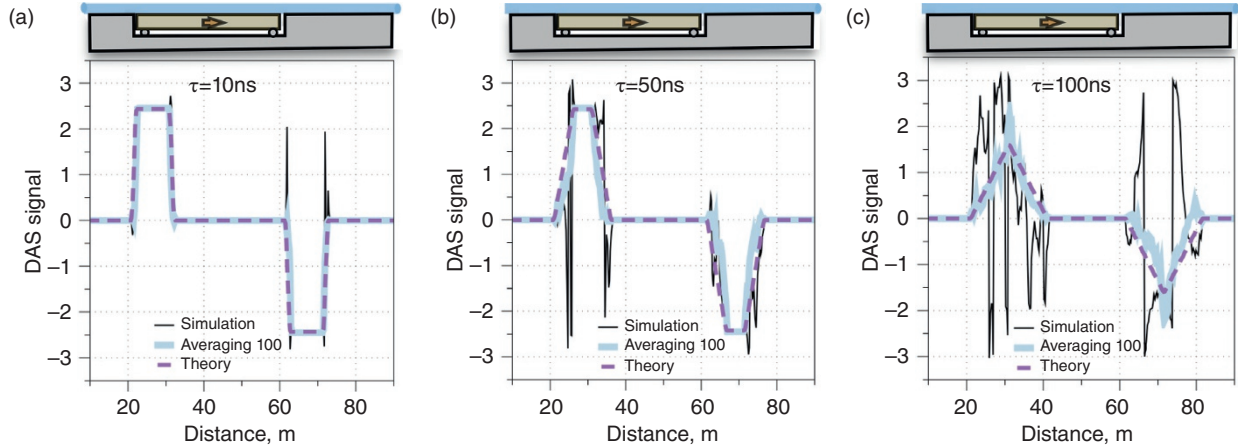


Figure 1.7 Comparison of DAS theoretical response (Equation 1.13) with simulation for a 3×3 coupler.

COTDR signal, which will be overlaid on the DAS signal with nonzero pulsewidth. This is a natural limit for increasing SNR by extending pulsewidth; we have a compromise between SNR and signal quality at around $L_0 = 2\tau$. Finally, we can expect that the theoretical expression (Equation 1.13) can be used for spatial resolution analysis for different phase recovery algorithms after a proper averaging.

1.1.4. DAS Dynamic Range Algorithms

An acoustic algorithm (Equation 1.15) transforms the DAS intensity signal into a phase shift proportional to fiber elongation value; a question then is how large can this phase shift be? An algorithm based on such ambiguous function as $\text{ATAN}(x)$ can give a result only inside a limited region. The classic approach to recover large phase changes is unwrapping: stitching together two consecutive points t and $t + \Delta t$ from different branches of signal (Itoh, 1982):

$$A_1(z, t) = F_S \frac{\partial}{\partial t} \text{UNWRAP}[\Phi(z, t)] \quad (1.17)$$

This unwrapping, or phase tracking, concept works only if the phase difference is inside two quadrants:

$$-\pi \leq \Phi(t + \Delta t) - \Phi(t) < \pi \quad (1.18)$$

Equation 1.17 makes it possible to measure significant fiber elongation, much longer than the wavelength. If the sampling rate $F_S = 1/\Delta t$ is higher than the acoustic frequency F , a larger acoustic amplitude can be integrated $A_0 F_S / 2F \approx 68\mu$ over time for $F = 50\text{Hz}$ and $F_S = 50\text{kHz}$. Moreover, even this value has improved, and

Equation 1.18 gives an idea of this. If the phase is a smooth function, we can differentiate in time $\Phi(t)$ before unwrapping. Then, the first differential linear term is removed, and condition becomes more relaxed:

$$-\pi \leq \Phi(t + 2\Delta t) - 2\Phi(t + \Delta t) + \Phi(t) < \pi \quad (1.19)$$

So, the second order tracking algorithm can be obtained by differentiating the signal before unwrapping:

$$A_2(z, t) = F_S \text{UNWRAP} \frac{\partial}{\partial t} [\Phi(z, t)] \quad (1.20)$$

Equation 1.20 has an analog in classical optics, where, instead of the wavefront phase gradient, the wrapped curvature of the wavefront can be unwrapped to increase the dynamic range (Servin et al., 2017). A comparison of these algorithms is presented in Figure 1.8 using modeling for a harmonic signal with a linearly increasing amplitude. It is visible that both algorithms can recover a significant phase range, but the second order tracking algorithm can deliver in excess of a 10 times larger dynamic range.

Theoretically, even higher order algorithms can be designed by repeating this process using higher order derivatives, but they are noisier as more points are involved in the calculation—as can be seen by comparing Equations 1.18 and 1.19. From a practical point of view, the proposed 1D (in time) unwrapping algorithms are error-free and simple enough to be implemented in real time. Potentially, noise immunity can be improved by transition to 2D (in time and distance) unwrapping, similar to that used in a synthetic aperture radar system (Ghiglia & Pritt, 1998). This solution can extract as much information about the phase as possible, but it is difficult to implement without post-processing.

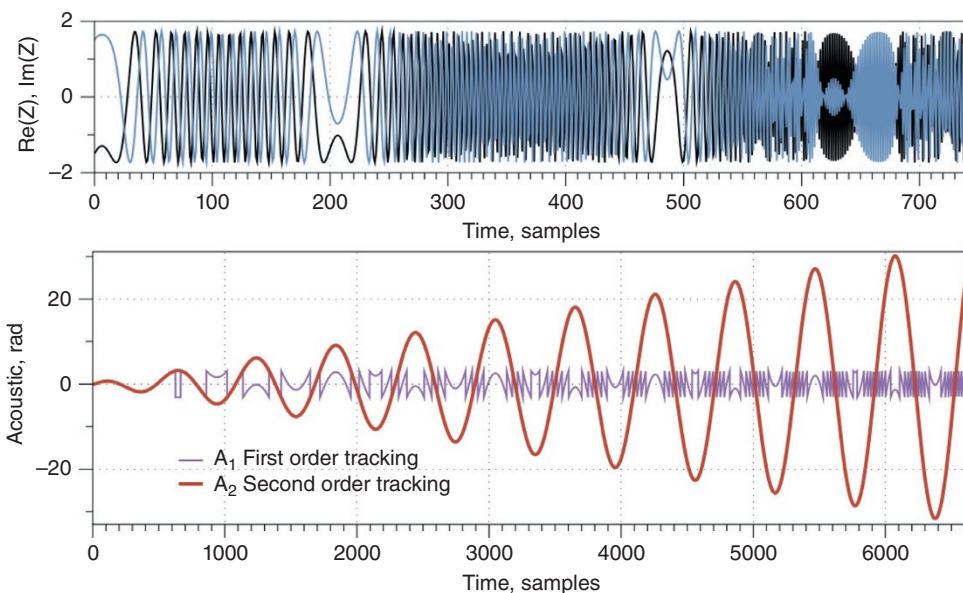


Figure 1.8 Comparison of first and second order tracking algorithms for DAS.

1.1.5. DAS Signal Processing and Denoising

In all phase-detection schemes, the change in optical phase between the light scattered in two fiber segments is determined, meaning we are measuring the deterministic phase change between two random signals. The randomness of the amplitude of the scattered radiation imposes certain limitations on the accuracy of the sensor, through the introduction of phase flicker noise. The source of flicker noise is an ambiguity: when the fiber is stretched, the scattering coefficient varies, and can become zero. In this case, the differential phase detector generates a noise burst regardless of which optical setup is used. The amplitude of such noise increases with decreasing frequency (as is expected for flicker noise) when the phase difference is integrated into the displacement signal.

From a quantum point of view, we need, for successive phase measurements, a number of interfering photon pairs scattered from points separated by the gauge length distance. In some “bad” points, there are no such pairs, as one point of scattering is faded. A natural way to handle this problem is to reject “bad” unpaired photons by controlling the visibility of the interference pattern. As a result, the shot noise can increase slightly as the price for the dramatic reduction of flicker noise. The rejection of fading points can be practically implemented by assigning a weighting factor to each measurement result and performing a weighted averaging.

This averaging can be done over wavelength if a multi-wavelength source is used. Alternatively, we can slightly sacrifice spatial resolution and solve the problem by denoising

using weighted spatial averaging (Farhadiroushan et al., 2010). The maximum SNR is realized when the weighting factor of each channel is chosen to be inversely proportional to the mean square noise in that channel (Brennan, 1959), meaning the squared interference visibility, V^2 , can be used for the weighting factor as:

$$\langle A(z) \rangle \approx \frac{A(z) \cdot V^2(z) \otimes p(z)}{V^2(z) \otimes p(z)} \quad (1.21)$$

The averaging function $p(z) = 5m$ should optimally be chosen to be compatible with the pulsewidth $\tau(z) = 50ns$, which should be around half the interferometer length $L_0 = 10m$. With this width of the averaging function, it has no significant effect on the spatial resolution of the DAS. Modeling with and without weighted averaging is presented in Figure 1.9, which demonstrates that significant noise reduction can be achieved. It should be noted that this noise reduction is particularly marked in comparison with the coherent OTDR response, by contrasting with Figure 1.5. Nevertheless, weighted averaging suppresses rather than completely removes the effect of flicker noise, and some channels still demonstrate excessive noise (in addition to shot noise). Hence, the response over all depths at a given time for Figure 1.9 will contain spikes for faded channels.

As is explored in Section 1.3, the problem of flicker noise can be overcome by introducing engineered bright scatter zones along the fiber with constant spatial separation and uniform amplitude. Such scatter zones also reflect more photons, and so improve the shot noise detection limitation. In addition, the use of such engineered

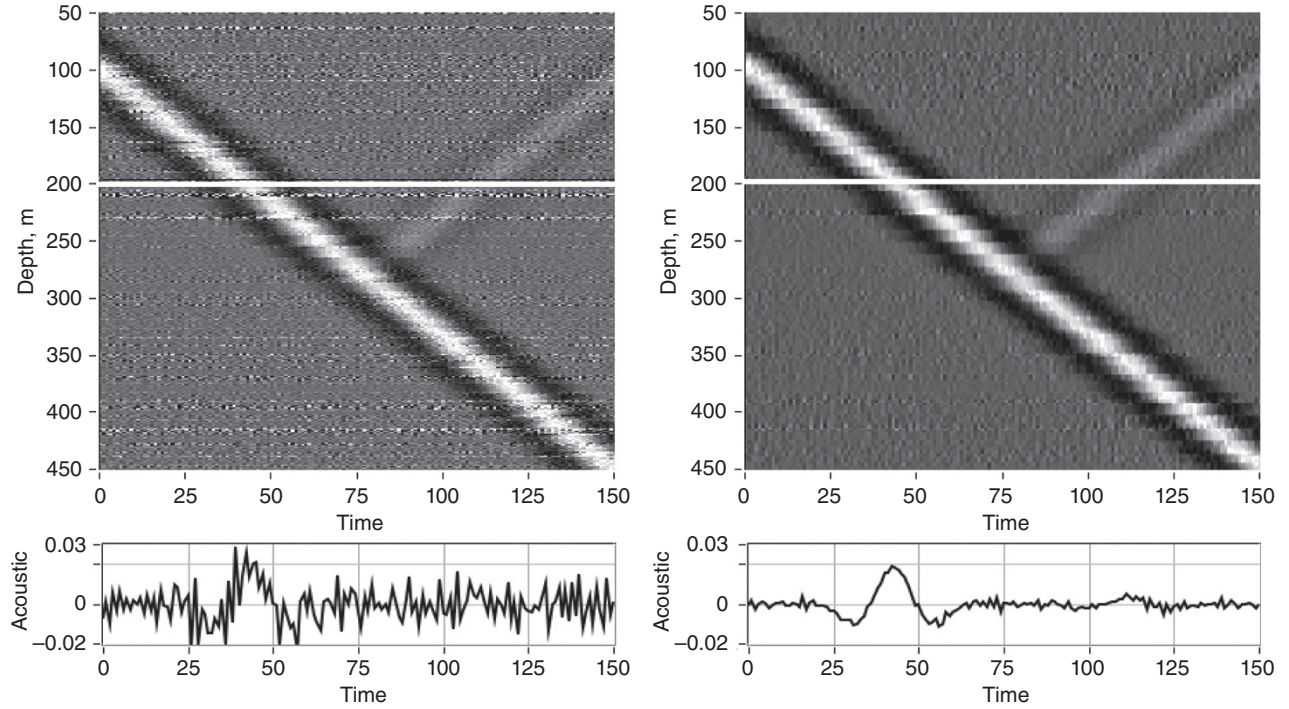


Figure 1.9 The left-hand panel shows modeling of raw DAS acoustic data (Equation 1.12); the right-hand panel shows the same shot with weighted averaging denoising (Equation 1.13) applied. The signals' cross-section along the white line is shown in the bottom panels in radians. The modeled source is shown in the right panel of Figure 1.5.

fiber allows the use of phase-detection algorithms with improved sensitivity and extended dynamic range.

1.1.6. Time Integration of DAS Signal

A DAS interrogator measures, in accordance with Equation 1.13, the speed difference between two sections of fiber that are separated by interferometer length L_0 (referred to also as the *gauge length*), as presented in Figure 1.10. In pulse-to-pulse consideration, the DAS response is linearly proportional to the fiber elongation averaged over the gauge length in the nanometer scale, or strain rate in the nanostrain per second scale. The consideration can also be extended to multiple pulses by time integration of the DAS signal. So, if fiber rests initially and ground displacement equals to zero $u(z, t_1) = 0$, then:

$$\int_{t_1}^{t_2} \langle A(z, t) \rangle dt = \frac{1}{A_0} \tau(z) \otimes [u(z, t_2) - u(z - L_0, t_2)] \quad (1.22)$$

meaning a time integrated DAS signal can be considered as an output of a huge caliper that is measuring fiber elongation between two points with sub-nanometer precision. This measuring principle is different from that of a geophone but is similar to an electromagnetic linear strain

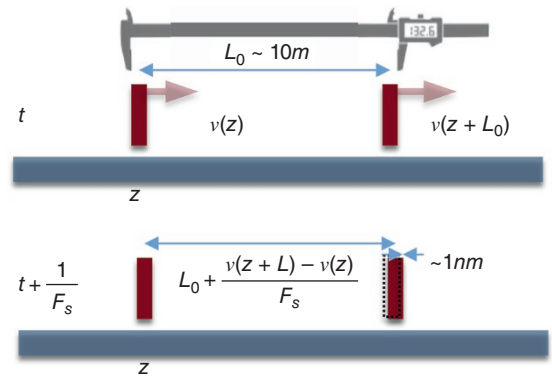


Figure 1.10 Illustration of two time-consecutive measurements when DAS output is proportional to fiber elongation between two probe pulses.

seismograph that can measure changes in distance between two points on the ground (Benioff, 1935).

1.2. DAS SYSTEM PARAMETERS AND COMPARISON WITH GEOPHONES

In this section, we consider how DAS parameters (such as spatial resolution), gauge length, frequency response,